

HOT WIRE SPATIAL RESOLUTION EFFECTS IN MEASUREMENTS OF GRID GENERATED TURBULENCE

A. Ashok, M. Hultmark, A.J. Smits

Department of Mechanical and Aerospace Engineering
Princeton University
Princeton, NJ
aashok@princeton.edu

S.C.C. Bailey

Department of Mechanical Engineering
Kentucky University
Lexington, KY

ABSTRACT

We use grid generated homogeneous isotropic turbulence as a benchmark flow to test the effects of spatial resolution on turbulence measurements with hot wires. The grid turbulence is generated in a low speed 0.6 m by 0.9 m closed circuit wind tunnel using a square mesh grid placed at the test section inlet. Measurements of the turbulence statistics and spectra downstream of the grid were made using hot-wires of varying length. An empirical correlation for the attenuation of the energy due to spatial filtering is constructed as a function of the parameter l/η . The effect of spatial filtering on the streamwise spectrum function is observed to extend to almost all wavenumbers, even those significantly lower than the length of the hot wire itself. It is shown that these grid turbulence results relate directly to the near-wall region of wall-bounded flows, where the effects of spatial filtering are most acutely felt.

INTRODUCTION

The motivation for this study comes from the need for highly resolved measurements of turbulent flows. Spatial filtering over some range of flow scales may occur when the length of the probe being used to measure the flow is larger than the size of the smallest scale. This subject has been the subject of considerable research, notably by Ligrani and Bradshaw (1987) and more recently by Hutchins et al (2009), Chin et al. (2010), Cameron et al. (2010) and Smits et al. (2011) for wall-bounded flows. These investigations focus on l^+ as the primary parameter governing spatial filtering, where $l^+ = lu_\tau/\nu$, l is the wire length, u_τ is the friction velocity, and ν is the kinematic viscosity, although Smits et al. identified the parameter l/y as an important factor outside the near-wall region. We aim to extend these approaches to

flows where it is not possible to define a viscous length scale ν/u_τ . In particular, we examine grid-generated turbulence where the relevant length scale for spatial resolution will be η , the Kolmogorov length scale.

Here, we use measurements of the grid-generated turbulence using a range of hot-wire sensor lengths, at a series of streamwise distances downstream of the grid, to investigate the impact of spatial filtering on measurements of the turbulence statistics. Points of comparison include streamwise evolution of the turbulence intensity as well as higher order statistics, the turbulent dissipation rate, and turbulent spectra. We also use this flow to assess the performance of a new Nano-Scale Thermal Anemometry Probe (NSTAP) (see Bailey et al. 2010 and Vallikivi et al. 2011). The NSTAP probe has a 60 μm long sensing element, measuring 100 nm by 2 μm in cross-section, with a frequency response that exceeds 150 KHz when operated in the constant temperature mode. For the purposes of the current experiment, the NSTAP forms the reference against which all other probes are measured against due to its superior spatial and temporal resolution.

EXPERIMENTS

In addition to the NSTAP, single normal hot wires are used in this investigation. Different lengths are achieved by etching Wollaston wire of 2.5 and 1.25 μm in diameter. The lengths used in this experiment range from 0.25 to 4 mm, corresponding to a range of l/d between 200 and 1600, where d is the wire diameter. The l/d ratio has classically been used to quantify end conduction effects, and Ligrani and Bradshaw's (1987) criterion for $l/d > 200$ has been adhered to in this experiment and therefore the data is assumed to be free of end conduction effects. Hultmark et al. (2011) have suggested a

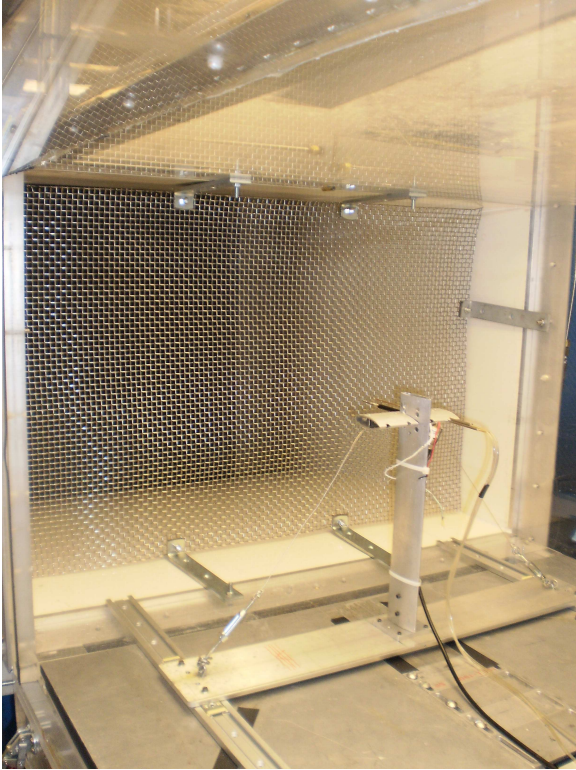


Figure 1. The square grid has a mesh size (M) of 0.25". The Pitot and hot wire probes are mounted on an airfoil which is itself connected to a dovetail traverse.

new criterion for end conduction effects in hot wires that takes into account the effect of wire thermal conductivity, Reynolds number and operating overheat ratio in addition to the length to diameter ratio. Their criterion, where it is required that $(\ell/d) \sqrt{4\gamma k_f Nu/k} > 14$, is also satisfied in the current investigation. γ is the resistance ratio, k_f [W/mK] is the thermal conductivity of the fluid, k is the thermal conductivity of the wire material and Nu is the Nusselt number. The hot wires are operated in a constant temperature circuit at high temperature overheat ratios, typically between 1.9 and 2.2. The frequency response as measured using a square wave test is summarized in Table 1 (end of paper) for the different wire lengths and freestream velocities. The 0.25 mm wire is run at a lower overheat of 1.6 in order to avoid drift since the 1.25 μ m diameter wire that is used to etch this shorter wire is sensitive to drift.

The grid turbulence is generated in a low speed 0.6 m by 0.9 m closed circuit wind tunnel using a 6.4 mm square mesh grid placed at the test section inlet which has a solidity of 46%. A traverse is used to move probes from between 20 and 90 mesh lengths, M , downstream of the grid. Figure 1 shows a schematic of the experimental setup. This allows for a range of Kolmogorov length scales for a given length of wire. The range of l/η obtained is between 0.1 and 70 for the two flow velocities used in this investigation (10 and 30 m/s).

RESULTS

Figure 2 shows the variance measured using a number of different wire lengths. The longer wires do not capture the small scale energies due to the spanwise averaging effect, but as the wire lengths decrease we see good agreement among the results. At 30 m/s the flow scales are small enough that even the shortest conventional wires are not able to match the true variance as measured by the NSTAP probe. Increasing the length of the wire increases the spanwise filtering, reducing the ability of the hot wire to resolve the small scale motions whilst simultaneously reducing the frequency response. Table 1 shows that the frequency response of the wires, when subjected to a square wave test in constant temperature mode, increases with mean velocity but not as quickly as the characteristic frequency of the turbulence u'/η . In the current work, we do not expect temporal filtering to be an issue, although in the extreme case of a 4 mm wire in a 30 m/s flow the reduced frequency response may be affecting the results.

It is well known that in the initial period of decay the variance decays according to a power law, so that

$$\frac{\frac{1}{2}\overline{u_i u_i}}{U_\infty^2} = A \left(\frac{x - x_0}{M} \right)^{-n} \quad (1)$$

where A is a constant that depends on the nature of the grid. The grid turbulence generated here shows good agreement with this power law, though the comparison depends strongly on the choice of the power law coefficients. The coefficients used here were, $A = 0.25$, $x_0 = 0$ and $n = 1.45$. Pope (2000) suggests that there is a wide scatter in the decay exponent n with values reported between 1.15 and 1.45. It appears that the grid turbulence generated in this study decays somewhat more quickly than in other studies. Perhaps the field at the early stages of development is not entirely homogeneous (it is well known that grid turbulence only tends to isotropy for $x/M \gg 10$) and inclusion of all downstream positions in plotting the decay law may skew the results. For the purpose of the present contribution, it appears that the grid produces a satisfactory approximation to a homogeneous and isotropic field.

The purpose of the grid turbulence was to generate a flow field with a wide range of scales. The largest scale in the flow is the streamwise integral length scale, L_x which is estimated as the area under the autocorrelation function as it evolves from a correlation coefficient of 1 to when the correlation is zero. The various estimates of the integral length scale surprisingly reveal an overestimation of the integral length scale by the larger probes particularly for the larger downstream distances. This suggests that the velocity time signal measured by the longer wires are correlated for longer than the unfiltered signal thereby yielding a greater area under the autocorrelation function, resulting in the larger than expected integral length scale. This may have been caused by the reduced frequency response particularly in the case of the 4 mm wire. However it is surprising that even the 0.5 mm wire so drastically overestimates (25 %) for the

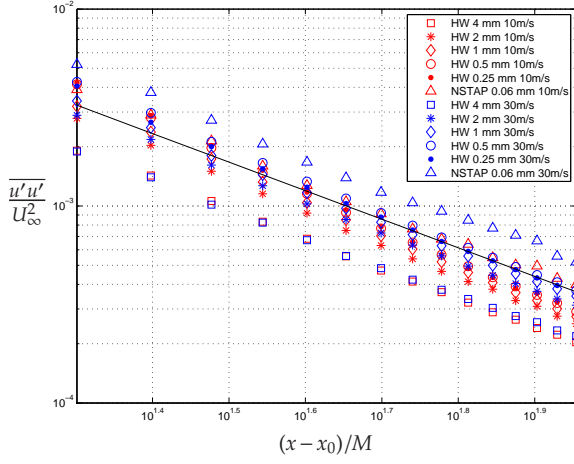


Figure 2. Streamwise turbulence intensity as a function of downstream distance. Measurements performed at 10 m/s are shown in red, 30 m/s profiles are in blue.

furthest downstream position. The low wavenumber filtering which was assumed to be a weak effect is in fact quite pronounced (see Figure 4) which might help explain why the Integral length scale is so affected by the filtering.

The smallest length scale is the Kolmogorov length scale, which was estimated using the slope of the turbulent kinetic energy profile because this is related to the dissipation rate through the simplified TKE equation for homogenous and isotropic flow. The dissipation rate as estimated by all the probes is shown in Figure 4. The higher velocity case clearly yields the greater dissipation of energy per unit mass due to the higher initial energy of the vortex shedding occurring as the flow is forced through the mesh. The discrepancy in the dissipation rate is higher than it might seem initially, as we are using a logarithmic scale. The estimated dissipation rate is considerably smaller for the larger probes as would be expected. Fortunately, this larger discrepancy in the dissipation rate is only partially transferred to the estimation of the Kolmogorov length scale since η is proportional to the 4th root of the dissipation rate.

As can be seen in Figure 5, η increases with downstream position, as expected. Note that the spatial filtering affects derived quantities such as the dissipation rate and therefore the Kolmogorov length scale. To quantify this further, Figure 6 shows the estimated Kolmogorov length scale as a function of l/η and we can see that despite some scatter in the data we can make out a clear trend with the η being consistently overestimated by the longer probes. This is naturally expected but it is interesting to note that discrepancies with respect to the NSTAP probe (again the reference) can be on the order of 10 % or more for conventional hot wire probes.

To quantify the spatial filtering effect, the mean square turbulence intensity at any one position may be normalized by its fully-resolved value. Here we assume that the NSTAP data represent the fully-resolved case. At 10 m/s the 0.25 mm wire data are in good agreement

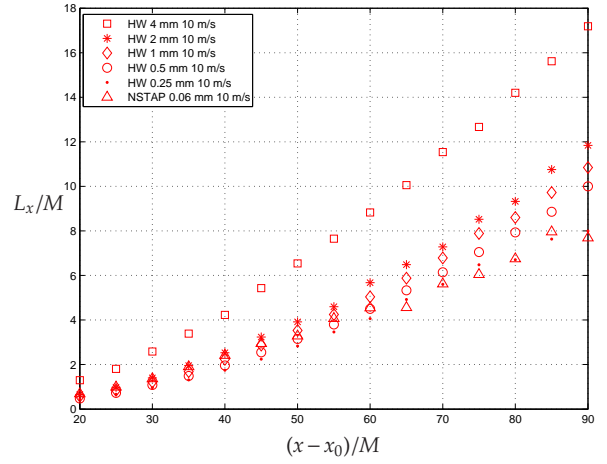


Figure 3. The Integral length scale, L_x estimated from the data taken using different probes.

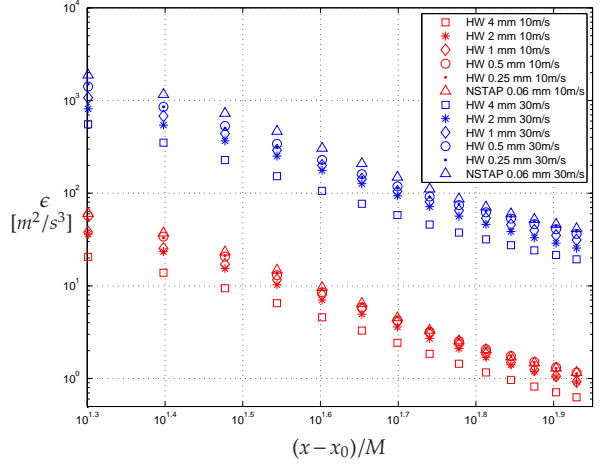


Figure 4. The dissipation rate, ϵ as a function of downstream position for 10 and 30 m/s.

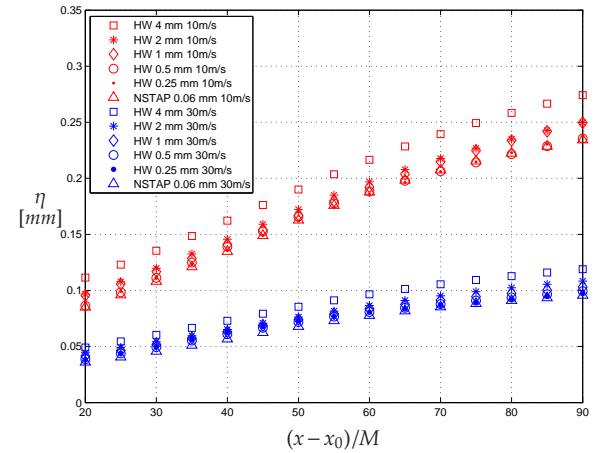


Figure 5. The estimated Kolmogorov length scale η as a function of downstream position again at 10 m/s and 30 m/s.

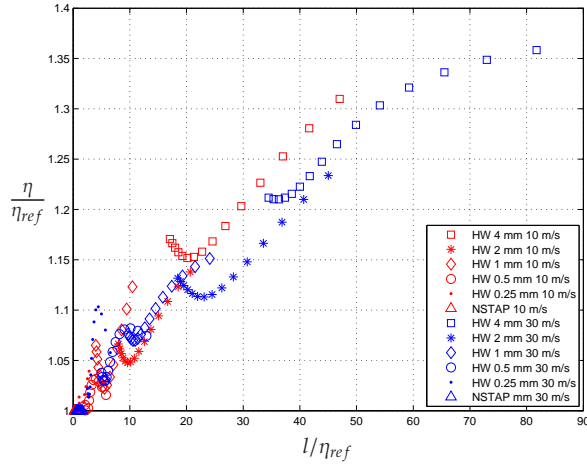


Figure 6. Ratio of measured η to the NSTAP measured value as a function of l/η .

with the NSTAP probe (0.06 mm) results, as can be seen in the spectra plotted in Figure 9. Figure 7 indicates how this ratio of measured to true variance varies with l/η . The loss of turbulent kinetic energy is monotonic with increasing l/η , and is well described by an exponential decay law.

In order to put these grid turbulence results in the context of wall-bounded turbulent flows where spatial resolution effects can be most acute, we consider the spatial correction based on the attached eddy hypothesis by Smits et al. (2011). The attenuation of the streamwise Reynolds stress due to spatial filtering is expressed in the following form by Smits et al. (2011),

$$\frac{\overline{\Delta u^2}^+}{\overline{u_m^2}^+} = g(l^+, z^+) = M(l^+)f(z^+). \quad (2)$$

Here, $\overline{\Delta u^2}^+$ is the difference between the measured and true variance and $\overline{u_m^2}^+$ is the measured variance. The attached eddy hypothesis of Townsend was used to define $f(z^+)$, and previously obtained experimental correlations and DNS data were used to construct an empirical correction for $M(l^+)$. Figure 8 compares the exponential decay correlation obtained from the grid turbulence results (see Figure 7) to the filtering predicted from Equation 2. The nine different profiles shown each correspond to a different value of l^+ . So having fixed l^+ we vary z^+ and obtained a correction for the variance. In order to compare this correction with the grid turbulence results we need a corresponding value for η^+ . Smits et al. used data from Hutchins et al. to estimate η^+ by integrating the 1-D streamwise spectra and assuming isotropy. In this way the correction can be plotted as a function of l/η . Each point then, on a given profile, corresponds to a different wall normal position ranging from $z^+ = 10$ to 100; each curve represents a different value of l^+ ranging from 10 and 100 to represent typical hot wire studies of wall-bounded flows. The lower values of $\frac{\overline{\Delta u^2}^+}{\overline{u_m^2}^+}$ corre-

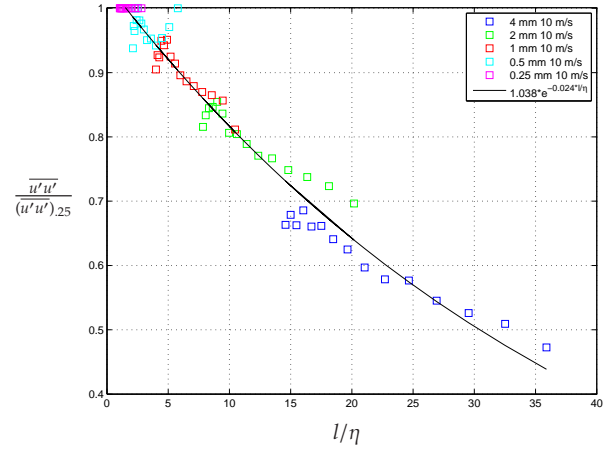


Figure 7. The variance for 10 m/s correlated as a function of l/η .

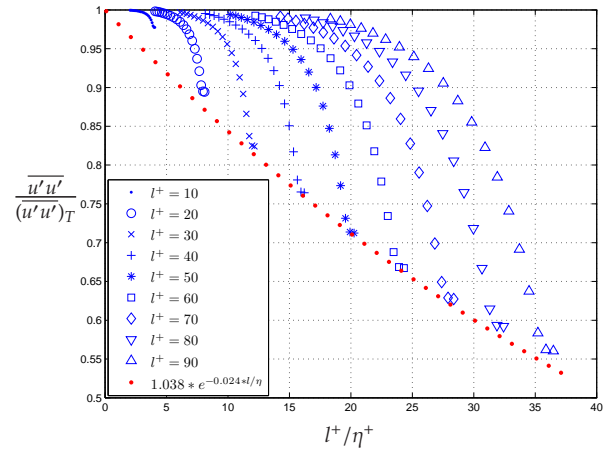


Figure 8. Comparison of the grid turbulence data (\cdot) with a correction function from Smits et al. (2011)

spond to lower values of z^+ . As can be seen there is a good agreement between the grid-turbulence based correction and the wall-bounded based correction for the near-wall region ($z^+ = 10$). This result suggests that filtering in the near wall region of a wall-bounded flow is remarkably similar to the filtering seen in grid turbulence. The anisotropy ratio in a wall bounded flow is highest near the wall and we would therefore expect correlations from an isotropic and homogeneous flow to be of questionable validity in the near wall region of a wall-bounded flow. It seems however that the ratio l/η scales the near wall variance very well and this seems to be a more important effect than the near-wall anisotropy.

Pre-multiplied spectra of the streamwise component of the velocity are shown in Figures 9 and 10 for a single downstream position (571 mm or 90M) at 10 and 30 m/s respectively. The spectra are presented in the Kolmogorov scaling so we expect that the form of the spectrum function is universal at high wavenumber. Deviations from a single curve may then be attributed to filtering effects and not other effects such as differing

initial or boundary conditions. At 10 m/s the differences between the wires are small enough such that the differences in the spectra are only just visible, but these differences are very much more evident at 30 m/s. In particular at high wavenumber a progressively more aggressive filtering of the energy by longer wires is visible. The spectra also reveal that the spatial filtering effects also occur at wavelengths much larger than the length of the hot wire. As Cameron et al. (2010) and Chin et al. (2010) and others have noted, this effect is due to the one-dimensional filtering of a three-dimensional signal. To show this effect more clearly the spectra are normalized by the results obtained using the NSTAP probe and are plotted as a function of the wavenumber only (see in Figure 11). So on the ordinate we see the factor by which any given probe filters the energy with respect to the NSTAP for every wavenumber. The filtering at high wavenumber is evident and obvious. In addition however, the low wavenumber filtering is actually quite significant with reported discrepancies on the order of 20% for 0.5 and 1 mm conventional hot wire probes. Here again we see that the higher the dissipation rate, the more the filtering high wavenumber end is affected by spanwise filtering.

We can take this a step further by examining what the effect of the filtering is on the proportion of the energy (area under the pre-multiplied spectra) that may be termed “high wavenumber.” The high wavenumber energy is taken to be the area under the pre-multiplied spectrum to the right (high wavenumber end) of the peak value measured using the NSTAP. Figure 12 shows the proportion of high wavenumber energy as a proportion of the total energy for different values of l/η . We see that the proportion of high wavenumber energy reduces as the extent of the spatial filtering grows. Clearly the proportion of high wavenumber energy is larger for the 30 m/s case but the rate at which this proportion reduces with wavenumber is approximately the same as for the 10 m/s case.

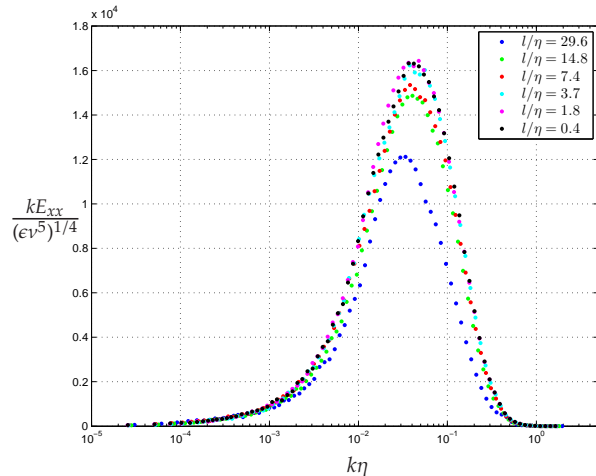


Figure 9. 1-D streamwise wavenumber spectra at 10 m/s (estimated from frequency spectra) plotted in Kolmogorov scaling. The scaling suggests that the scaled spectrum should be a universal function of $k\eta$.

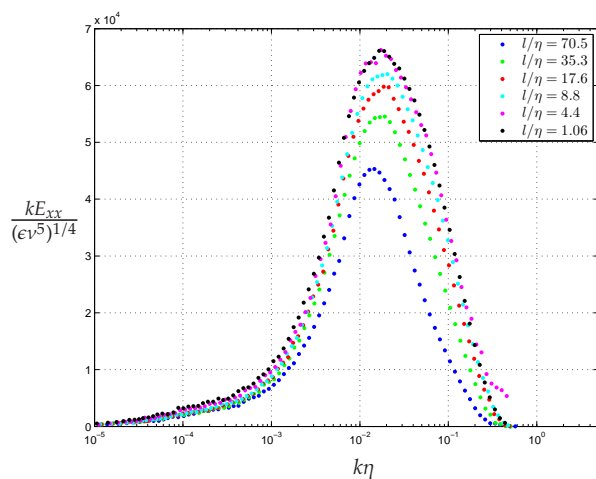


Figure 10. 1-D streamwise wavenumber spectra at 30 m/s (estimated from frequency spectra) plotted in Kolmogorov scaling showed separately to the 10 m/s case for clarity.

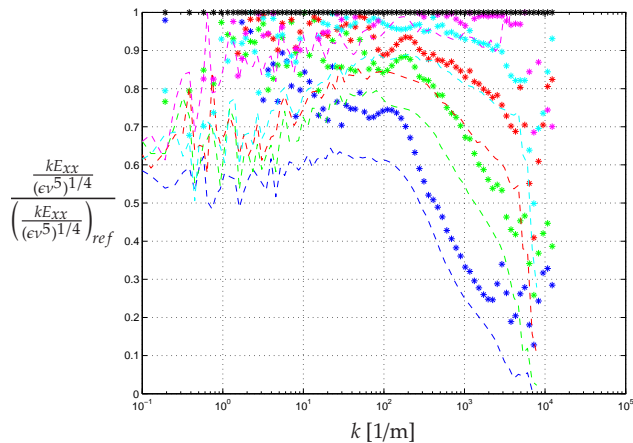


Figure 11. Spectra normalised by the NSTAP for 10 m/s (solid lines) and 30 m/s (dashed lines) for the different l/η ratios. Colour convention same as Figure 9 and Figure 10.

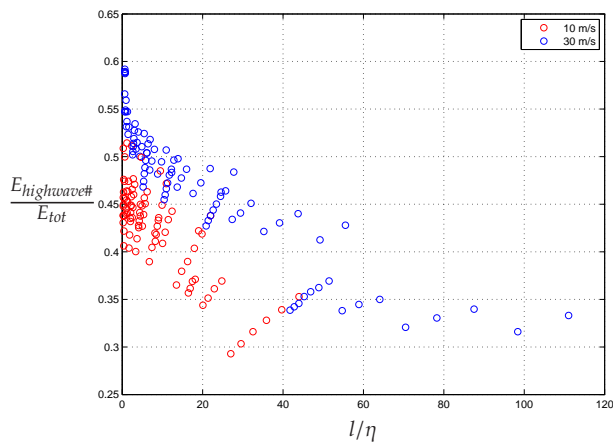


Figure 12. Proportion of high wavenumber energy as a fraction of total energy for the different l/η ratios

CONCLUSION

Grid turbulence was used to study the effects of spatial filtering on turbulence measurements. These effects were clearly visible in the variance, and derived quantities such as estimates of the dissipation rate and the Kolmogorov length scale were also found to be compromised by the spatial filtering. It was found that the parameter l/η correlated the variance data very well and the variation was found to be described well by an exponential function. Good agreement was found between the wall bounded flow correction proposed by Smits et al. (2011) in the near wall region and the spatial filtering

correlation found here.

The spectra showed that the effect of spatial filtering is felt at almost all wavenumbers, as noted by previous authors. At the higher velocity the spectra reveal more aggressive filtering of the energy at high wavenumber compared to low wavenumber. By plotting the high wavenumber energy as a function of l/η it is possible to see that the rate at which the high energy contributions are filtered with l/η is about the same for both the 10 m/s and 30 m/s cases even if the fraction of high wavenumber energy is higher for the 30 m/s case.

REFERENCES

- M. Vallikivi, M.Hultmark, S.C.C. Bailey, A.J. Smits, 2011, "Turbulence measurements in pipe flow using a nano-scale thermal anemometry probe" Experiments in Fluids (submitted)
- Bailey, S., Kunkel, G., Hultmark, M., Vallikivi, M., Hill, J., Meyer, K., Tsay, C., Arnold, C. & Smits, A. 2010 "Turbulence measurements using a nanoscale thermal anemometry probe." Journal of Fluid Mechanics.
- Cameron, J. D., Morris, S. C., Bailey, S. C. C. & Smits, A. J. 2010 "Effects of hot-wire length on the measurement of turbulent spectra in anisotropic flows". Measurement Science and Technology.
- Chin, C. C., Hutchins, N., Ooi, A. S. & Marusic, I. 2009 "Use of direct numerical simulation (DNS) data to investigate spatial resolution issues in measurements of wall-bounded turbulence." Measurement Science and Technology.
- Ligrani, P.M. & Bradshaw, P. 1987, "Spatial resolution and measurement of turbulence in the viscous sub-layer using subminiature hot-wire probes." Experiments in Fluids.
- Hutchins N., Nickels T. B., Marusic I. & Chong M.S. 2009 "Hot-wire spatial resolution issues in wall-bounded turbulence." Journal of Fluid Mechanics.
- A.J. Smits, J. Monty, M. Hultmark, S.C.C. Bailey, N. Hutchins & I. Marusic. 2011 "Spatial resolution correction for wall-bounded turbulence measurements. Journal of Fluid Mechanics"

ACKNOWLEDGEMENTS

This work was supported by ONR Grant N00014-09-1-0263 (Program Manager Ron Joslin) and NSF Grant CBET-1064257 (Program Manager Henning Winter).

The authors would also like to thank Margit Vallikivi for generously providing her NSTAPS and to Mike Vocaturo and Glenn Northey for their technical assistance.

Table 1. TSFP-7 table.

	0.25 mm	0.5 mm	1 mm	2 mm	4 mm
Temperature overheat ratio	1.6	2.1	2	1.9	1.85
Characteristic frequency, $\sqrt{u'u'}/\eta$ @ 10 m/s	6 KHz	6 kHz	5 kHz	4.5 kHz	3.2 kHz
Frequency response @ 10 m/s	90 kHz	50 kHz	40 kHz	30 kHz	15 kHz
Characteristic frequency, $\sqrt{u'u'}/\eta$ @ 30 m/s	42 KHz	40 kHz	35 kHz	30 kHz	22 kHz
Frequency response @ 30 m/s	120 kHz	75 kHz	60 kHz	50 kHz	25 kHz